

EVALUATION OF NOSEBOOM SENSORS CORRECTION COEFFICIENTS OF THE FLYING HELICOPTER SIMULATOR FHS

Antje Dittmer

antje.dittmer@dlr.de

German Aerospace Center, DLR

Lilienthalplatz 7, D-38108 Braunschweig, Germany

ABSTRACT

The EC135 Flying Helicopter Simulator (FHS) of DLR is equipped with noseboom mounted sensors to enable measurements relatively unperturbed by rotor downwash effects. Remaining downwash disturbances on the static and dynamic pressure and the airflow angles are compensated for with correction coefficients, derived with a variant of the Simultaneous Calibration of Aircraft Data System (SCADS) technique. The correction coefficients depend on the sensor reference values as well as on the accuracy of wind estimations which are necessary in the absence of measured wind. The quality of the correction coefficients derived using this estimated wind is evaluated by comparing the difference in wind estimation from three different objective functions and two different optimization routines. Additionally, position error correction (PEC) tower flyby maneuvers with accurate wind measurements close to the helicopter flight path are used to verify the results obtained via the SCADS windbox technique.

1 INTRODUCTION

The German Aerospace Center (DLR) operates a modified EC135 as the Flying Helicopter Simulator (FHS), figure 1.



Figure 1: The Flying Helicopter Simulator

The basic air data system (ADS) of the FHS uses a pitot tube to measure dynamic and static pressure. Due to the pitot tube being mounted below the helicopter, the accuracy of the measurement decreases with decreasing airspeed as the rotor downwash influences the ADS pressure signals. Therefore, a noseboom equipped with a pitot tube and two airflow angle vanes is mounted on the FHS. These sensors need to be calibrated in-flight. An in-flight calibration, a so called dynamic calibration, of the statically calibrated sensors is necessary to compensate remaining downwash disturbances. At the National Research Council (NRC), Canada, the Simultaneous Calibration of Aircraft Data System (SCADS) technique has been developed [1–3]. It allows to simultaneously calibrate the pitot sensor and the airflow angles. This technique uses special windbox maneuvers that combine accelerations, decelerations and beta-sweeps in a box pattern.

The SCADS method has been successfully applied for calibrating the noseboom air data systems of the NRC research airplane and helicopters [1–3] and of the DLR research airplane ATTAS [4]. As the FHS noseboom, including the pitot tube and angle of attack and sideslip angle sensors, is identical to the one of the NRC helicopter, the SCADS calibration method is used for the FHS noseboom as well. The calculation of correction coefficients for the FHS noseboom sensors via optimization of the noseboom pressure based airspeed, using the SCADS method as well as using a classical flight path reconstruction, is discussed in [5] and [6].

This paper starts with a description of the noseboom sensors to be calibrated. A short description of the differential GPS (DGPS) and the wind measurement sensors is provided. Both are used to generate the reference signals. INS/GPS, ADS, and radar altitude sensor measurements are used to validate these reference values. The flight test used to estimate the wind, the SCADS windboxes, are presented, as well as tower flybys with measured wind. The physical equations applied to obtain the noseboom correction coefficients are summarized. Different optimization methods and objective functions for the derivation of the estimated wind and correction coefficients are discussed. The correction coefficients, obtained with estimated wind are validated with airspeeds derived via GPS and wind measurements.

2 HELICOPTER SENSORS

For the dynamic calibration of the noseboom pitot tube and angle vanes, the following high precision measurements are used to derive the necessary reference data:

- DGPS measurements
- wind measurements for tower flyby maneuvers

The DGPS airspeed measurements are compared to the INS/GPS data which have been shown by application of flight path reconstruction to yield accurate results [6]. The airspeed and height above ground for the calibration flight test are verified by comparing them to data from the following measurements, respectively:

- INS/GPS measurements for ground speed
- ADS measurements for airspeeds between 40 and 110 kt
- radar altitude measurements

The instrumentation used in the calibration is described in more detail in the following subsections. In subsection 2.1 the noseboom sensors for the measurements to be calibrated are described. The DGPS and wind measurement sensors used as reference values are presented in subsections 2.2 and 2.3. The INS/GPS, ADS, and radar sensors used to validate the reference DGPS values are described in subsections 2.4, 2.5, and 2.6.

2.1 Noseboom System

The FHS noseboom, depicted in figure 2, is equipped with a pitot static system measuring dynamic and static pressure and two airflow angle vanes.



Figure 2: FHS noseboom with airflow and pitot sensors

The pitot tube is mounted at the front end of the noseboom. According to its sensor specification [7], the installed head orifices allow for pressure measurement errors to be essentially zero up to angles of attack or sideslip of $\pm 40^\circ$ at velocities from 25 kt to 200 kt. The vane used for angle of attack measurements is mounted horizontally to the left side. The other vane, which measures sideslip, is fixed vertically to the boom. It has to be noted that the sideslip vane does not directly measure the sideslip angle. Instead, the flank angle is measured. This is due to the fact that the vanes measure the angle between the longitudinal and vertical respectively lateral airspeed component. Mathematical equations relating flank angle, angle of attack and sideslip angle are given in section 4. Airspeed-dependent calibration curves both for airspeed and airflow angles, obtained from wind tunnel tests, are included in [7]. The manual proposes a linear calibration curve for the correction of the airspeed error. In [5] it is shown that the pressure error increases quadratically with increasing airspeed. The dynamic pressure error is thus linearly dependent on the dynamic pressure which corresponds to the observations described in [3, 4].

2.2 DGPS System

The DGPS system used at DLR on the FHS is the system Sharpe XR6 of the company Symmetricom Ltd [8]. During all flight tests recorded, care is taken that real-time kinematic (RTK) GPS is always operational. RTK is a differential technique which uses pseudo-range as well as carrier phase measurements to compute the position of the mobile receiver relative to the base station. This highest accuracy mode relies on having differentially corrected carrier phase measurements available to achieve position accuracies down to the low centimeter range for the GPS North and East components as well as for the GPS altitude component [8].

2.3 Wind Measurement

For the flyby maneuvers, a wind measurement system of the company Thies Clima is used, that consists of an anemometer and weather vanes. The system measures the wind speed and direction at 10 m height with a sampling interval of one second [9]. The weather vanes allow for a speed accuracy of 0.6 kt. The wind direction measurement allow for an accuracy of 2.5° . The wind measured during the flight tests did not exceed 10 kt. As the runway and the airport field are flat surfaces and the flybys are performed at heights between 5 and 20 m, it can be assumed that the wind measured at a height of 10 m is a good representation of the wind acting on the helicopter.

2.4 Honeywell INS/GPS System

The accuracy of the INS/GPS ground speed data of the Honeywell system was validated via flight path reconstruction [6]. The INS/GPS signal is compared to data from the DGPS system. The standard deviation of the error between INS/GPS and DGPS speed does not exceed 0.4 kt in all three speed components. The mean value of the error is smaller than 0.04 kt in all components. In [4] the measured data are post-processed with a Kalman filter to obtain INS based GPS measurements for a flight path reconstruction (FPR). For the FHS, this Kalman filtering is already done inside the INS/GPS system. A calculation using INS/GPS data is performed to derive pressure and airflow correction coefficients. The correction coefficients and estimated wind components derived with INS/GPS are compared to results obtained with DGPS values. The difference in estimated wind data did not exceed 0.3 kt. The difference in the pressure and the two airflow multiplication coefficients is not larger than 10^{-5} . The difference in the pressure bias correction coefficient is not larger than 10^{-5} Pa. The difference in the two airflow bias correction coefficients is not large than 10^{-5} rad. It is thus concluded that the influence of the difference between the two GPS systems can be neglected. The DGPS altitude is used as the reference altitude, see subsection 2.6. The DGPS ground speed components are taken as the reference ground speed components to use as few sensors for the reference data as possible.

2.5 Air Data System

The FHS helicopter is equipped with an air data system ADS 3000 from Sextant Avionique which is part of the standard EC-135 equipment [13]. The system measures the static and dynamic pressure as well as the static air temperature. From these measurements, the indicated, calibrated and true airspeed are derived as well as the total air temperature. This is done by applying speed dependent correction coefficients to the measured pressures and deriving the airspeed from the corrected pressures. It will be shown in section 5 that the indicated values agree well with INS/GPS measurements subtracted by the respective wind components for airspeeds higher than 40 kt.

2.6 Radar Measurement

For an evaluation of the quality of the DGPS height, the signals are compared to the radar height. For this purpose the height is to be given as height above sea-level in the earth-fixed coordinate system. The tower flybys were performed on the relatively flat surface of the runway. The height above sea level is therefore assumed to be constant with $z_{GND} = 89.9$ m, the height of the runway of the Braunschweig airport.

The tower flyby flights at low speed were performed within a distance of 10 m to the ground over the runway. These tests are primarily flown to find the lowest airspeed at which the noseboom pressure port still yields usable measurements. They are shortly described in section 3 of this paper and in more detail in [5]. They can be used as well to test the accuracy of the DGPS height, as the radar measurements are very accurate within this range, a distance to the ground smaller than 10 m, to a flat surface like the runway. The mean difference between DGPS and radar height is 0.63 m for the tower flybys with low distance to the runway, and a maximum difference in altitude of 3 m.

According to its manual, the DGPS height is accurate in the low centimeter range if RTK-GPS is active. This accuracy could not be proven by comparison to the radar sensor, from the results an accuracy within 1 m is assumed. Still, as the exact height of the ground level is unknown, the difference between radar and DGPS sensor might be due to changes in the height of the ground rather than DGPS measurement errors. The DGPS height is therefore used as the reference altitude for the noseboom calibration.

3 FLIGHT MANEUVERS

Two different flight test maneuvers are used for the FHS noseboom calibration:

- SCADS windbox, reference airspeed derived with GPS and estimated wind
- tower flyby, reference airspeed derived with GPS and measured wind

The maneuvers are shortly summarized here. They are described in more detail in [5].

3.1 SCADS windbox

The SCADS windbox, first presented in [3], consists of a series of different maneuvers flown in a box pattern. For the FHS noseboom calibration the same extended windboxes as depicted in figure 3 are flown.

The maneuver definition for the six sides is as follows:

1. low constant airspeed V_{lo} , accelerate by 20 kt at corner to V_{hi}
2. high constant airspeed $V_{hi} = V_{lo} + 20$ kt, decelerate 5 kt at corner to V_{m1}
3. beta sweeps at constant intermediate airspeed $V_{m1} = V_{lo} + 15$ kt, decelerate at corner to V_{m2}
4. beta sweeps at constant intermediate airspeed $V_{m2} = V_{lo} + 10$ kt, decelerate at corner to V_{m3}
5. maximum climb power (MCP) climb at intermediate airspeed $V_{m3} = V_{lo} + 5$ kt
6. autorotation descent at intermediate airspeed $V_{m3} = V_{lo} + 5$ kt

The windbox pattern has been repeated with the starting airspeed V_{lo} varying from 20 to 90 kt with a step width of 10 kt. The SCADS windbox maneuvers are hence flown at eight different airspeed variations. Four of these maneuvers are flown twice to obtain redundant data, resulting in a total of twelve different SCADS windboxes used for correction coefficient calculation. This approach leads to a wide range of different airspeeds in steady flight. The climb maneuvers are used for constant negative angles of attack, the descent maneuvers are used for constant positive angles of attack. The duration of the windbox legs is 60 s; the windbox legs' length varies accordingly from 600 to 3000 m. The height above ground varies between 400 and 1000 m. At the time of the flight tests no exact airspeed indicator for airspeeds below 30 kt was available. Hence, the airspeed of the first windbox was closer to 30 than 20 kt.

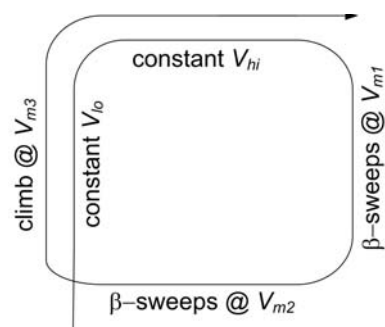


Figure 3: SCADS windbox maneuver

3.2 Tower Flyby Maneuver

To be able to obtain the position error of the static pressure measurement also by classical methods, flybys over the runway are performed. The flight test is described in [2]: At a reference point with known GPS coordinates a 'baseline position' and a pressure at sea level (QNH) are recorded. Then several tower flyby nap-of-the-earth flights are performed to get measurements for a calibrated point of the air data system. The flybys are performed at an altitude of 10 m above ground and

velocities between 20 and 100 kt. To minimize wind influence, all flybys are flown up and down the runway. Angle of sideslip variations via beta-sweeps is integrated during some of the flybys. In order to check if the angle of attack correction coefficients are valid, some acceleration and deceleration maneuvers near the tower are included, with airspeed variation between 20 and 110 kt in one recorded flight test. The SCADS windbox tests are used to calibrate the sensors for the speed range between 30 and 110 kt.

To be able to determine the minimum airspeed at which the noseboom sensors still yield valid airspeed measurements, some more low-speed flybys are performed. During these tests, a GPS-equipped car sets the reference speed by driving along the runway at constant speed while the helicopter follows at a constant distance. These pace car flybys are performed from 5 km/h (2.7 kt) to 50 km/h (27 kt). As this flight test was performed under very calm weather conditions, not only the helicopter ground speed but also the resulting airspeed is nearly constant.

4 NOSEBOOM CALIBRATION EQUATIONS

For the calibration, the true static and dynamic pressure and the true airflow angles have to be derived from GPS and wind data. For the tower flybys, measured wind is available. With measured wind, the correction coefficients can be calculated analytically. For the SCADS windboxes no measured wind is available, and the wind has to be estimated. Physical relations presented in this section are used to estimate the wind and to calculate the correction coefficients in order to minimize the difference between the true values and the corrected noseboom measurements.

The measured angle of attack α_i and the measured flank angle β_{Fi} are corrected with their respective bias correction coefficients C_{A0} and C_{B0} , and their multiplication correction coefficients C_{A1} and C_{B1} , to the corrected noseboom angles α_{NB} and $\beta_{F,NB}$:

$$\begin{aligned} (1) \quad \alpha_{NB} &= C_{A0} + C_{A1}\alpha_i, \\ (2) \quad \beta_{F,NB} &= C_{B0} + C_{B1}\beta_{Fi}. \end{aligned}$$

The difference between the reference dynamic pressure P_d and the dynamic pressure measured at the noseboom P_{di} is calculated as the noseboom position error correction, PEC :

$$(3) \quad PEC = P_d - P_{di}$$

Generally, the static pressure measured by the pitot static system differs from the free stream pressure. This difference is primarily dependent on sensor location and vehicle airspeed. The pressure measurement error is called position error correction (PEC). It corrects errors introduced by local airflow at the position of the sensor. The PEC is used as reference value to which the corrected noseboom PEC_{NB} is fitted in a least squares sense, see subsection 4.1. The PEC_{NB} is calculated with

the bias and multiplication correction coefficients C_{P0} and C_{P1} :

$$(4) \quad PEC_{NB} = C_{P0} + C_{P1}P_{di}.$$

The corrected dynamic noseboom pressure $P_{d,NB}$ is then calculated as:

$$(5) \quad P_{d,NB} = C_{P0} + (1 + C_{P1})P_{di}.$$

If the airspeed is calculated using measured wind, the calculation of the correction coefficients can be broken down as follows:

1. airspeed as difference between GPS ground speed and wind speed
2. calculation of static pressure based on measured GPS altitude and QNH pressure
3. air density based on calculated static pressure and measured temperature
4. calculation of dynamic pressure from GPS based air density and true airspeed
5. calculation of pressure correction coefficients C_{P0} and C_{P1}
6. transformation of airspeed components from geodetic to body-fixed system
7. transformation of airspeed components from the reference position to the noseboom position
8. calculation of angles of attack and sideslip from GPS and wind based airspeed components
9. calculation of airflow angle correction coefficients C_{A0} , C_{A1} , C_{B0} , and C_{B1}

The correction coefficients depend on the wind. If no measured wind is available (SCADS windboxes), an optimization routine has to rerun these steps iteratively to calculate the wind components which minimize an objective function. The wind is changed in order to minimize the difference between reference and corrected noseboom measurements. The differences between reference and corrected noseboom values are weighted with weighting factors and added to different weighted sums. Differences considered in different objective functions take into account airflow angles, dynamic pressure, airspeed components and altitude. The different steps are explained below with the formulas used to derive the physical values taken from [1–4, 12].

The inputs to the physical model used to create the reference values for the measured noseboom pressures and airflow angles are:

- 3 GPS ground speed components (V_{GN} , V_{GE} , V_{GD}) and GPS altitude (h_G)
- 3 Euler angles (Φ , Θ , Ψ), 3 angular rates (p , q , r)
- air temperature T
- current QNH pressure P_{QNH} at sea level as provided by the airport tower
- 3 wind speed components (V_{WN} , V_{WE} , V_{WD}), either measured (tower flybys) or estimated (SCADS windboxes)

The noseboom inputs to be corrected are its indicated static pressure P_{si} , its indicated dynamic pressure P_{si} , its indicated angle of attack α_i and its flank angle β_{Fi} .

4.1 Pressure Sensor Correction Coefficients

The airspeed is calculated as the difference of the INS/GPS speed and the wind speed. From the ground speed components V_{GN} , V_{GE} , and V_{GD} in the north-east-down earth coordinate system, the wind speed components V_{WN} , V_{WE} , and V_{WD} are subtracted to obtain the helicopter airspeed components in the earth coordinate system:

$$(6) \quad V_N = V_{GN} - V_{WN},$$

$$(7) \quad V_E = V_{GE} - V_{WE},$$

$$(8) \quad V_D = V_{GD} - V_{WD}.$$

The wind components are estimated to optimize the minimization criteria. For the tower flybys the estimated wind is compared with wind measured near the tower. From the airspeed components the true airspeed V_{TAS} is calculated as:

$$(9) \quad V_{TAS} = \sqrt{V_N^2 + V_E^2 + V_D^2}.$$

The static pressure can be derived from the GPS altitude of the helicopter, the current pressure at sea level, the so called QNH pressure P_{QNH} and the corresponding temperature T_{QNH} :

$$(10) \quad P_s = P_{QNH} \left(1 + \frac{dT}{dh} \frac{h}{T_{QNH}} \right)^{\frac{n}{n-1}}.$$

The pressure at sea level P_{QNH} is provided by the tower, $dT/dh = -0.0065$ K/m is the temperature coefficient of the standard atmosphere and $n = 1.235$ the polytropic exponent.

The temperature T_{QNH} at sea level corresponding to this pressure can be calculated via the physical dependency of density and pressure of ideal gases [12]:

$$(11) \quad T_{QNH} = T_0 \left(\frac{P_{QNH}}{P_0} \right)^{\frac{n-1}{n}}.$$

Here, the pressure $P_0 = 101325$ Pa is the standard pressure at sea level at an altitude of $h_0 = 0$ m. The following ideal gas equations are applied to derive equation (11), with the measured temperature T and the density values ρ , ρ_{QNH} and ρ_0 corresponding to the static pressure P_s at flight level, the actual static pressure at sea level P_{QNH} and the standard static pressure at sea level P_0 :

$$(12) \quad \rho = \frac{P_s}{RT},$$

$$(13) \quad \frac{P_{QNH}}{P_0} = \left(\frac{\rho_{QNH}}{\rho_0} \right)^{\frac{1}{n}}.$$

where $R = 287.0529$ J/kgK is the gas constant.

The dynamic pressure is calculated via the density ρ and the true airspeed V_{TAS} :

$$(14) \quad P_d = 0.5\rho V_{TAS}^2.$$

Using this reference PEC , based on P_d , see equation (3), the bias C_{P0} and the multiplication correction coefficient C_{P1} can be calculated. The PEC

is approximated in a least squares sense by PEC_{NB} . The difference between all measurements of PEC and PEC_{NB} recorded during one flight test maneuver is $r_P = [r_P(t_0), r_P(t_1), \dots, r_P(t_n)]^T$ with:

$$(15) \quad \begin{aligned} r_P(t_0) &= PEC(t_0) - (C_{P0} + C_{P1}P_{di}(t_0)) \\ r_P(t_1) &= PEC(t_1) - (C_{P0} + C_{P1}P_{di}(t_1)) \\ &\dots \\ r_P(t_n) &= PEC(t_n) - (C_{P0} + C_{P1}P_{di}(t_n)) \end{aligned}$$

with the flight recording starting time t_0 and its end time t_n . The data is recorded at $n + 1$ discrete time instants t_i , with the index i varying from 0 at the start of the recording to its end n at the time t_n . An underlined value \underline{x} denotes in this work a vector containing $n + 1$ measurements from $x(t_0)$ to $x(t_n)$.

For the calculation of the coefficients C_{P0} and C_{P1} the pseudo-inverse of the matrix $\underline{A}_P = [\underline{1}, \underline{P}_{di}]$ is used:

$$(16) \quad \begin{aligned} \underline{A}_P [C_{P0}, C_{P1}]^T &= \underline{PEC} \\ \Rightarrow [C_{P0}, C_{P1}]^T &= (\underline{A}_P^T \underline{A}_P)^{-1} \underline{A}_P^T \underline{PEC} \end{aligned}$$

The vector $\underline{1}$ is an $n + 1$ -size column vector with every element equal to 1. Applying the correction coefficients from (16) to the equation system (15) results in the smallest possible value for $\underline{r}_P^T \underline{r}_P$. Unlike in [1,2] the coefficients are therefore not derived via an optimization routine but calculated analytically based on the estimated wind, while in [1,2] both the wind components and the correction coefficients are estimated by an optimization routine. The approach chosen in this paper has the advantage of less optimization parameters if the wind is to be estimated.

4.2 Airflow Sensor Correction Coefficients

For the calculation of the reference airflows, the DGPS and wind based airspeed components V_N , V_E , and V_D from (6), (7), and (8) are transformed into the body-fixed coordinate system via a concatenation of rotations by the Euler angles Ψ , Θ , and Φ . The airspeed components resulting from this transformation are the airspeed components u , v , and w in the body-fixed system.

These airspeed components are transformed to the noseboom. The airspeed components u , v , and w are given at a so-called general control point, GCP. It is defined as origin of the body-fixed system instead of the center of gravity, as the center of gravity varies with loading conditions. The linear transformation to the noseboom location is given in [3]. It is a sum of the airspeed vector acting at the GCP and a vector product of the three angular rates p , q , and r and the distance between the GCP and the noseboom center in the x -, y -, and z -direction of the body-fixed coordinate system:

$$(17) \quad u_{GCP@NB} = u - ry_{GCP,NB} + qz_{GCP,NB},$$

$$(18) \quad v_{GCP@NB} = v + rx_{GCP,NB} - pz_{GCP,NB},$$

$$(19) \quad w_{GCP@NB} = w - qx_{GCP,NB} + py_{GCP,NB}.$$

The two airflow vanes shown in figure 2 measure the indicated angle of attack α_i and the flank angle β_{Fi} at the noseboom. It has to be noted that the sideslip vane does not measure the sideslip angle, but instead the flank angle. The true airflow angle α and flank angle β_F at the

noseboom are defined based on airspeed components at the noseboom:

$$(20) \quad \alpha = \tan^{-1} \frac{w_{GPS@NB}}{u_{GPS@NB}},$$

$$(21) \quad \beta_F = \tan^{-1} \frac{v_{GPS@NB}}{u_{GPS@NB}}.$$

The sideslip angle β has to be calculated from the flank angle and the angle of attack. It is defined as the angle between the airspeed component $v_{GPS@NB}$ and the magnitude of the airspeed $V_{GPS@NB}$, with the airspeed magnitude defined as

$$(22) \quad V = \sqrt{u^2 + v^2 + w^2},$$

the reference sideslip angle at the noseboom equals:

$$(23) \quad \beta = \sin^{-1} \frac{v_{GPS@NB}}{V_{GPS@NB}}.$$

It can also be calculated from α and β_F via

$$(24) \quad \beta = \tan^{-1}(\tan(\beta_F)\cos(\alpha)).$$

Linear correction coefficients are introduced to model the influence of the downwash. The true angle of attack and the true flank angle can be approximated by the corrected noseboom airflow angles α_{NB} and $\beta_{F,NB}$:

$$(25) \quad \alpha_{GPS@NB} \approx \alpha_{NB} = C_{A0} + C_{A1}\alpha_i,$$

$$(26) \quad \beta_{F,GPS@NB} \approx \beta_{F,NB} = C_{B0} + C_{B1}\beta_{Fi}.$$

where α_i and β_{Fi} are the noseboom indicated values of angle of attack respectively flank angle. The correction coefficients C_{B0} , C_{A0} , C_{B1} and C_{A1} are calculated analytically, using the pseudo-inverse of $\underline{A}_\alpha = [\underline{1}, \alpha_i]$ and the pseudo-inverse of $\underline{A}_\beta = [\underline{1}, \beta_{Fi}]$, respectively. From these corrected noseboom angles α_{NB} and $\beta_{F,NB}$, the corrected noseboom sideslip angle β_{NB} is calculated, as described in equation (24).

4.3 Reference and Corrected Noseboom Data

The wind is estimated based on a best fit between reference data and corrected noseboom data. Above, the calculation of a reference PEC and reference airflow angles α and β and the corresponding corrected noseboom values PEC_{NB} , α_{NB} , and β_{NB} is described.

Reference airspeed components $u_{GPS@NB}$, $v_{GPS@NB}$, and $w_{GPS@NB}$ are calculated in subsection 4.2. The airspeed components based on the corrected noseboom airflow angles and dynamic pressure are:

$$(27) \quad V_{NB,TAS} = \sqrt{2(P_{di} + PEC_{NB})/\rho_{NB}},$$

with the noseboom measurement dependent density ρ_{NB} calculated as:

$$(28) \quad \rho_{NB} = \frac{P_{s,NB}}{RT}.$$

The corrected noseboom airspeed components are calculated as:

$$(29) \quad u_{NB} = V_{NB,TAS}\cos\alpha_{NB}\cos\beta_{NB},$$

$$(30) \quad v_{NB} = V_{NB,TAS}\sin\beta_{NB},$$

$$(31) \quad w_{NB} = V_{NB,TAS}\sin\alpha_{NB}\cos\beta_{NB}.$$

A reference altitude h is directly provided by the DGPS altitude. The altitude h_{NB} is calculated based on the corrected static noseboom pressure $P_{s,NB}$. The true static pressure P_s is given as the measured static pressure P_{si} subtracted by the PEC [1–4], the corrected static noseboom pressure $P_{s,NB}$ is therefore calculated by subtracting PEC_{NB} :

$$(32) \quad P_s = P_{si} - PEC,$$

$$(33) \quad P_{s,NB} = P_{si} - PEC_{NB}.$$

The corresponding altitude h_{NB} is calculated by inserting the corrected static noseboom pressure $P_{s,NB}$ into equation (10).

5 OBJECTIVE FUNCTION FOR WIND ESTIMATION

The wind can be optimized to minimize the objective function $J_{h,V}$ presented in [1], a weighted sum of ground speed component errors and altitude error. In [1–3] it is mentioned that the coefficients of

1. the position error correction equation, C_{P0} , and C_{P1}
2. the airflow angle model, C_{A0} , C_{A1} , C_{B0} , and C_{B1} ,
3. the wind model, V_{WN} , V_{WE} , and V_{WD}

are varied by the Direct Search Complex algorithm [1–3]. As it is possible though to calculate the correction coefficients analytically depending on the wind components, only the three wind components V_{WN} , V_{WE} , and V_{WD} are varied to get a best fit between the reference values and the corrected noseboom measurements if the wind for one windbox is estimated. From the approach taken in [1–3] the number of optimization parameters is thus reduced from nine to three.

In [5] it is discussed that the concatenations of four windboxes flown with different starting airspeeds V_{Io} leads to a considerable reduction in the standard deviation of the calculated pressure correction coefficients. The first and the third windbox concatenation set include windboxes with starting velocities V_{Io} of 20 kt, 40 kt, 60 kt and 80 kt. The second set concatenates windboxes with starting velocities V_{Io} of 30 kt, 50 kt, 70 kt and 90 kt. The 12 downward wind components V_{WD} , calculated for the 12 windboxes flown, are estimated to be close to zero. Hence for the windbox concatenations of four windboxes, only the horizontal wind components V_{WN} and V_{WE} are estimated. During one windbox the wind is considered to be constant in this approach as well. As for each of the four windboxes of the three windbox concatenation sets two wind components are calculated, this leads to a total of eight parameters to be estimated: $V_{WN,WBox1}$, $V_{WN,WBox2}$, $V_{WN,WBox3}$, $V_{WN,WBox4}$, $V_{WE,WBox1}$, $V_{WE,WBox2}$, $V_{WE,WBox3}$, $V_{WE,WBox4}$. The approach using three windbox concatenation sets à four windboxes is called SCADS2, the approach using 12 windboxes is called SCADS1 approach. Further details are given in [5], in which the two methods are compared to the classic flight path reconstruction technique. In [1, 2] the objective function used is a weighted sum of errors in ground speed components and altitude. In [3]

the objective function used is a weighted sum of the errors in ground speed components. Airspeed components are compared in this work rather than ground speed components in order to reduce the number of calculation steps. In order to calculate the reference airflow angles which are necessary to calculate the airflow correction coefficients C_{A0} , C_{B0} , C_{A1} and C_{B1} , a transformation from the earth-fixed coordinate system into the body-fixed system is necessary. The reference airspeed components and the corrected noseboom airspeed components are compared to avoid the transformation of the body-fixed airspeed components derived from corrected noseboom data into the earth-fixed coordinate system. As the difference between ground speed and airspeed components is equal to the wind components, the choice of difference in airspeed rather than ground speed as the minimization objective should not influence the result of the wind estimation.

While different objective functions are used in [1,2] compared to [3], the influence of this difference of objective functions, and hence the choice of the objective functions, is not discussed. Here, the wind components are optimized with respect to three different objective functions. It is evaluated if the choice of objective function influences the resulting estimated wind. Only objective functions are considered here whose weighted sum contain summands dependent on the corrected noseboom pressures as well as on the airflow angles.

In [5], it was tested how well the reference airspeed components could be matched with the corrected noseboom dynamic pressure and airflow angles. It is demonstrated that the thus obtained corrected noseboom airspeed is a good match to the reference airspeed for airspeeds between 16 and 110 kt.

The difference between reference and noseboom measurement based airspeed components is calculated as:

$$\begin{aligned}\Delta_u &= [\underline{u}_{GPS@NB} - \underline{u}_{NB}]^T [\underline{u}_{GPS@NB} - \underline{u}_{NB}], \\ \Delta_v &= [\underline{v}_{GPS@NB} - \underline{v}_{NB}]^T [\underline{v}_{GPS@NB} - \underline{v}_{NB}], \\ \Delta_w &= [\underline{w}_{GPS@NB} - \underline{w}_{NB}]^T [\underline{w}_{GPS@NB} - \underline{w}_{NB}], \\ \Delta_V &= \sqrt{\Delta_u + \Delta_v + \Delta_w}.\end{aligned}$$

If only the airspeed components are matched to the reference values, the following objective function is to be optimized:

$$(34) \quad J_V = x_V \Delta_V = x_V \sqrt{\Delta_u + \Delta_v + \Delta_w}$$

with $x_V = 1$ s/m. This dimensionless objective function, a sum of the airspeed components measured in m/s multiplied with x_V , resembles the weighted sum of ground speed components used in [3]. It has to be noted that the mean difference in GPS height and noseboom height derived via J_V does not exceed 2 m for the SCADS wind-box runs, which is relatively small. This is due to the fact that the correction of the static pressure, and hence for the altitude measurement, is optimized as well if the following modeling assumption is true:

$$PEC = P_d - P_{di} = P_{si} - P_s.$$

It is investigated though how much the height difference can be further decreased by the application of $J_{h,V}$. The height difference between reference height based on GPS data and the height calculated from corrected noseboom measurements is directly included in the optimization function $J_{h,V}$. The second objective function chosen for the current investigation, $J_{h,V}$, is a weighted sum of the altitude error in 1/m ($x_h = 1$ /m) and the airspeed error in m/s ($x_V = 1$ s/m):

$$(35) \quad J_{h,V} = x_h \Delta_h + x_V \Delta_V$$

The difference Δ_h between reference and noseboom measurement based height is calculated as:

$$\Delta_h = \sqrt{[\underline{h} - \underline{h}_{NB}]^T [\underline{h} - \underline{h}_{NB}]}.$$

The third function used is the weighted sum $J_{P,\alpha,\beta}$ of the differences between reference position error correction PEC , angle of attack α , and flank angle β_F and their respective approximations PEC_{NB} , α_{NB} and $\beta_{F,NB}$:

$$(36) \quad J_{P,\alpha,\beta} = x_P \Delta_P + x_\alpha \Delta_\alpha + x_\beta \Delta_\beta$$

with

$$\begin{aligned}\Delta_P &= \sqrt{[PEC - PEC_{NB}]^T [PEC - PEC_{NB}]}, \\ \Delta_\alpha &= \sqrt{[\alpha - \alpha_{NB}]^T [\alpha - \alpha_{NB}]}, \\ \Delta_\beta &= \sqrt{[\beta_F - \beta_{F,NB}]^T [\beta_F - \beta_{F,NB}]},\end{aligned}$$

with $x_P = 10^{-5}$ 1/Pa and $x_\alpha = x_\beta = 180^\circ/\pi$ 1/deg, with the airflow data provided in radians. This objective function is chosen for comparison as it directly measures the quality of the linear approximations of the position error correction and the airflow angles.

6 OPTIMIZER FOR WIND ESTIMATION

In [1] the weighted sum of the height and ground speed differences is minimized by the Direct Search Complex algorithm. The Direct Search Complex algorithm is a global optimizer, whose boundary conditions have to be given. It is investigated if an optimization with a local optimization routine is sufficient or if a global optimizer has to be applied.

For a convex problem, i.e. a problem with only one optimum, a local optimizer is always sufficient. A local optimizer can be applied as well if the starting point of the problem can be chosen to enable the optimizer to find the solution from this starting point. The flight tests were performed under calm weather condition, hence it was assumed that for the estimation of the three wind components, V_{WN} , V_{WE} , and V_{WD} , the results obtained with a local optimization method would closely resemble the ones derived with a global optimizer. This assumption is verified. The following optimizers are chosen:

The applied local optimizer is the Nelder-Mead simplex, described in [13] and implemented in the Matlab function `fminsearch.m`. The global optimizer is the differential evolutionary algorithm, with the Matlab implementation `devec3.m` described in detail in [14].

The optimization iterations of the Nelder-Mead simplex can be summarized as follows:

Simplex Set-up: A starting point $\underline{x}_{0,0}$ is chosen, in this case the starting point $\underline{x}_{0,0} = [V_{WN,0}, V_{WE,0}, V_{WD,0}]'$ is chosen to equal the wind measured at the tower at the beginning of the flight. A simplex near the initial starting point is set up. A simplex consists of $N+1$ vertex points for an N -dimensional problem, i.e. for the SCADS1 method a tetrahedron for a three-dimensional problem with the vertex points of the first optimization iteration $\underline{x}_{0,1}, \underline{x}_{1,1}, \underline{x}_{2,1}, \underline{x}_{3,1} \in \mathbb{R}^3$.

Order: The values of the objective functions are calculated for each point of the simplex and ordered according to their value; in this example this might result in $J(\underline{x}_{0,1}) > J(\underline{x}_{1,1}) > J(\underline{x}_{2,1}) > J(\underline{x}_{3,1})$. The center point $\underline{x}_{M,1}$ of all points except for the point with the largest objective function is calculated; in this case the center of the triangle $\underline{x}_{M,1}$, with the points $\underline{x}_{0,1}, \underline{x}_{1,1}$, and $\underline{x}_{2,1}$.

Reflection: The point with the largest objective function $\underline{x}_{3,1}$ is reflected on the center point $\underline{x}_{M,1}$, the resulting point $\underline{x}_{3,r}$ is calculated as

$$\underline{x}_{3,r} = \underline{x}_{M,1} + \rho_{NMS}(\underline{x}_0 - \underline{x}_{3,1})$$

with the reflection factor set to $\rho_{NMS} = 1$. If the objective function $J(\underline{x}_{3,r})$ is smaller than the second largest objective function of a point of the last generation but larger than the objective function of the best point of the last generation, a new simplex is setup and the reflection is repeated. Here the simplex of the second generation would consist of $\underline{x}_{0,1}, \underline{x}_{1,1}, \underline{x}_{2,1}, \underline{x}_{3,r}$.

Expansion: If the reflection results in a smaller objective function than the one of the originally best point, the simplex of the next generation is calculated by expanding the vertex point

$$\underline{x}_{3,e} = \underline{x}_{M,1} + \chi_{NMS}(\underline{x}_0 - \underline{x}_{3,1})$$

with the expansion factor set to $\chi_{NMS} = 2$. If $J(\underline{x}_{3,e})$ is smaller than $J(\underline{x}_{3,r})$, the step is repeated. Else, a simplex is setup with $\underline{x}_{3,r}$ as one of the vertex points.

Contraction: If the objective function $J(\underline{x}_{3,r})$ is larger than the largest objective function $J(\underline{x}_{3,1})$ of the previous generation, then a new simplex is obtained by replacing the worst point of the previous generation with the contracted point $\underline{x}_{3,c}$. The contracted point is calculated as:

$$\underline{x}_{3,c} = \underline{x}_{M,1} + \psi_{NMS}(\underline{x}_0 - \underline{x}_{3,1})$$

with the contraction factor set to $\psi_{NMS} = 0.5$. If the objective function value $J(\underline{x}_{3,c})$ is smaller than the second largest objective function of the previous generation $J(\underline{x}_{2,1})$, a new simplex is set up. If it is larger than $J(\underline{x}_{2,1})$, all but the best point $\underline{x}_{0,1}$ are changed by reducing their distance to the center points of the simplex.

Reduction: For all but the best point successor points are calculated by reducing their distance to the center

point $\underline{x}_{M,n}$ of the n^{th} iteration. In the considered example the vertex points of the simplex of the second iteration are then calculated as:

$$\underline{x}_{i,2} = \underline{x}_{M,1} + \sigma_{NMS}(\underline{x}_0 - \underline{x}_{i,1}), i \in 1, 2, 3$$

with the reduction factor $\sigma_{NMS} = 0.5$.

Break condition: The break conditions are the number of simplexes exceeding $n = 600$, or the absolute difference between the best simplex vertex points smaller than 0.0001, or the absolute improvement in the objective function smaller than 0.0001.

The algorithm is deterministic, a given starting point always results in the same solution, if the set-up of the initial simplex from a starting point is a deterministic one. If the distance between the vertex points of the initial simplex is too small, the algorithm will converge to a local minimum near the initial simplex. With the distance between the initial simplex vertex points chosen to be too large, the runtime of the algorithm is unnecessarily long. Here, as the wind components acting on the helicopter are assumed to be relatively similar to the ones measured at the airport tower, the default values for the simplex set-up are used, which lead to a thorough search of the near environment of the initial value $\underline{x}_{0,0}$. The first vertex point is set to equal the initial value $\underline{x}_{0,1} = \underline{x}_{0,0} = [V_{WN,0,0}, V_{WE,0,0}, V_{WD,0,0}]'$. The three other vertex points $\underline{x}_{i,1}, i \in 1, 2, 3$ are calculated as

$$\underline{x}_{i,1} = 0.05 \text{ m/s} + \underline{x}_{i-1,1}, i \in 1, 2, 3.$$

If the assumption is true that the wind is relatively similar to the initial wind assumption, the wind estimated with this algorithm is a good approximation of the actual wind. However, should the wind differ largely from this assumption, the small difference in the initial vertex points might lead the algorithm to converge to a local minimum. It will be shown that for the SCADS1 approach these default values of the Nelder-Mead simplex lead to the same solution as a global optimizer. Neither the step size nor the initial size of the simplex sides are chosen too small. A heuristic global optimizer is used to validate that the solution found by the local optimizer is the global optimum.

The heuristic optimizer applied is a differential evolutionary algorithm, a vector population based stochastic optimization method. The basic idea behind it is to have several starting points $\underline{X}_0 = [\underline{x}_{1,0}, \underline{x}_{2,0}, \dots, \underline{x}_{i,0}]$ rather than just one $\underline{x}_{0,0}$. Each starting point \underline{x} is considered to be an individual of a population \underline{X} of i individuals, which develops over n iterations, often called generations. Its parameters $\underline{x}_{i,n} = [x_{1,i,n}, x_{2,i,n}, \dots, x_{k,i,n}]$ are its 'genes'. Similar to a real population, the individuals of one generation \underline{X}_N produce children, the generation \underline{X}_{N+1} , following certain rules, i.e. they are changed and recombined to form new solution points. The calculation steps of the evolutionary algorithm are therefore the following:

Evolutionary algorithm population set-up: The number of individuals as well as the boundaries of the

initial population are chosen. The maximum iteration number and other exit conditions have to be defined a-priori. Here, with the number of genes $k = 3$ equal to the number of wind components $V_W = [V_{WN}, V_{WE}, V_{WD}]$, the number of individuals is set to $i = 30$ and the maximum number of iterations to $n = 100$ for the SCADS1 approach. For the SCADS2 approach, with the number of genes $k = 8$, the number of individuals is set to $i = 30$ and the maximum number of iterations to $n = 200$. No other exit condition than the number of iteration is given. Although a range for the first generation of individuals has to be defined, the algorithm is able to search for solutions outside these original boundaries [14]. For the wind estimation for the SCADS wind box flights, the boundaries for north and east wind components V_{WN} and V_{WE} are both set to -10 m/s and 10 m/s (19.4 kt). The vertical wind component V_{WD} is set to vary between -1 m/s and 1 m/s (1.94 kt) and is found to be close to zero for all flight data recorded during the SCADS windboxes.

Order: The value of the objective function of each individual of a generation is calculated. The chances of an individual of the n^{th} generation \underline{X}_N to be used as a parent of individuals of the next generation \underline{X}_{N+1} is larger, if its objective function is small i.e. closer to the optimum.

Crossover and recombination: A certain number of children is calculated by recombinations of the genes of the parent generation. The recombination value is set to $\gamma_{CR} = 0.8$. Thus most of the children are calculated by recombination. Recombination allows a thorough search between the points of the parent generation. The best l individuals of the parent generation are used in the next generation as well, a method called 'elitism'. In this case, the best individual is saved, i.e. $l = 1$. Saving the best individual guarantees that information once found is not lost. By setting l to a small number as $l = 1$, allows for the rest of the population to vary. By keeping l small, the total number of individuals can be relatively small as well.

Mutation: A certain number of children are calculated by variation of the 'genes', here the wind components, of the parent generation. This variation is called mutation. How many children are defined by this variation, called 'mutation', is fixed in the mutation ratio, which is here set to $\gamma_M = 0.4$. During the iteration, the mutation ratio is reduced by a shrinking factor. At the beginning of the optimization the probability of mutation is high to allow the algorithm to search for solutions outside the initial boundaries. The probability of mutation is reduced during the iteration to enable the algorithm to search the neighborhood of points with small cost function more thoroughly.

Break condition: The break condition is exceeding the maximum number of iterations, set to $n = 100$ for the SCADS1 and to $n = 200$ for the SCADS2 approach.

The wind components optimized with this global optimization routine are in a second optimization step

used as initial values of the Nelder-Mead simplex optimizer. This is called hybrid optimization. It is difficult to evaluate whether the wind calculated with the differential evolutionary algorithm is actually the global optimum, or if the solution close to the best point of the last iteration is better. The Nelder-Mead simplex optimizer is due to its systematic reduction of the simplex size more suitable to search the neighborhood of an initial point thoroughly than the evolutionary algorithm.

The wind components V_{WN} , V_{WE} , and V_{WD} for the 12 SCADS1 windboxes are thus estimated with a global optimizer, a concatenation of evolutionary algorithm and Nelder-Mead simplex, and a local optimizer, the Nelder-Mead simplex. It will be shown in section 7 that for the calculation of the three wind components the Nelder-Mead simplex converges to the same solution as the evolutionary algorithm.

The wind components $V_{WN, WBox1}$, $V_{WN, WBox2}$, $V_{WN, WBox3}$, $V_{WN, WBox4}$, $V_{WE, WBox1}$, $V_{WE, WBox2}$, $V_{WE, WBox3}$, $V_{WE, WBox4}$ for the SCADS2 windbox sets are estimated with the two optimizers. It will be demonstrated in section 7 that for the starting values chosen to be the ones provided by the tower, the Nelder-Mead simplex does not converge to the same solution as the concatenation of evolutionary algorithm and Nelder-Mead simplex. The results obtained with the evolutionary algorithm/Nelder-Mead simplex and the SCADS2 approach closely resemble the results obtained with the SCADS1 approach. Details are given in subsection 7.2.

7 WIND COMPONENTS ESTIMATION

The dependency of the estimated wind parameters on the objective function and on the optimizer used are discussed in subsections 7.1 and 7.2 respectively.

7.1 Comparison of Objective Functions

The SCADS windbox maneuvers are flown at eight different airspeed variations see subsection 3.1. Four of these maneuvers are flown twice. This leads to a total of 12 windboxes, resulting in 12 sets of correction coefficients for the SCADS1 approach.

The values of the wind components V_{WN} , V_{WE} , and V_{WD} estimated to be constant during one windbox are shown in figure 4 for each of the twelve windboxes. The resulting wind speeds shown are obtained with the combination of evolutionary algorithm and the Nelder-Mead simplex optimizer. The displayed wind components minimize the objective functions J_V , $J_{h,V}$, and $J_{P,\alpha,\beta}$. It can be seen from figure 4 that the differences between the wind components estimated for each single run are relatively small. The exact mean values and standard deviations of the difference between the 12 wind components estimated with J_V , $J_{h,V}$, and $J_{P,\alpha,\beta}$ listed in table 1.

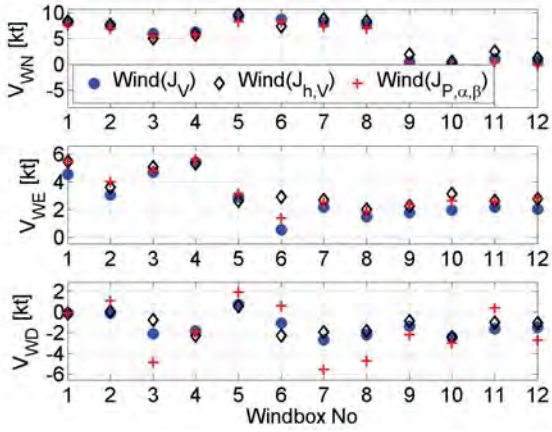


Figure 4: Constant wind components estimated for the 12 windboxes, optimal regarding J_V , $J_{h,V}$, and $J_{PEC,\alpha,\beta}$

In table 1 the difference between the 12 north wind components, estimated with J_V and concatenated to the vector $\underline{V}(J_V)$, and the vector $\underline{V}(J_{h,V})$, containing 12 wind components estimated with $J_{h,V}$, is denoted ΔV_{WN} $J_V, J_{h,V}$. The other five difference vectors are determined and named accordingly. Their mean values and standard deviations are listed below.

		mean [kt]	std [kt]
ΔV_{WN}	$J_V, J_{h,V}$	-0.20	0.84
	$J_V, J_{P,\alpha,\beta}$	0.69	0.16
ΔV_{WE}	$J_V, J_{h,V}$	-0.64	0.67
	$J_V, J_{P,\alpha,\beta}$	-0.52	0.30
ΔV_{WD}	$J_V, J_{h,V}$	-0.19	0.65
	$J_V, J_{P,\alpha,\beta}$	0.41	1.72

Table 1: Difference between wind components, derived with different objective functions

The difference in wind speed is below the highest measurement accuracy of the ADS, which amounts to a maximum error of 2 kt at airspeeds higher than 50 kt [11].

Two reasons lead to the use of different objective functions: It is tested if similar wind components are estimated independent of the objective function. The assumption that any objective function implicitly weighting the difference between reference values for dynamic pressure and airflow angles will lead to similar estimated wind components is verified. This strongly suggests that the wind components found by the optimizer are indeed the best approximation of the wind acting on the helicopter.

The second reason for testing and comparing different objective functions is to test if including the altitude difference explicitly in the objective functions will lead to a better fit between reference altitude and noseboom based altitude. As the first aim of showing that almost the same wind is estimated independent of the objective function is achieved, both the increase in difference between airspeed as well as the decrease in altitude will be relatively small. The differences in airspeed $\Delta_V/(n+1)$ and altitude $\Delta_h/(n+1)$ to the reference values at each step of the optimization iteration is shown in figure 5 for the fifth SCADS windbox with $V_{lo} = 70$ kt. The differences Δ_V and Δ_h are divided by the number of

measurements $n+1$ to allow for a clearer interpretation of the data, independent of the number of measurements. The fifth SCADS windbox is chosen since the differences for the estimated wind components are largest for this windbox, see figure 4.

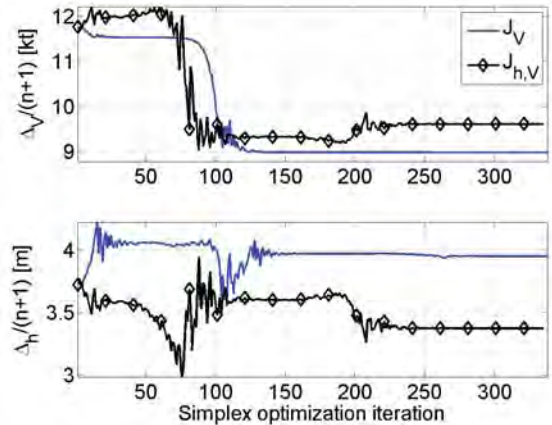


Figure 5: Difference between reference and corrected noseboom values at each simplex iteration for J_V and $J_{h,V}$

In the first subfigure, the difference in airspeed Δ_V between reference data and corrected noseboom data in kt is shown. In the second subfigure the difference in altitude corresponding to each iteration step is displayed. The optimization algorithm used is the Nelder-Mead simplex optimizer. The decrease in altitude difference, resulting from the use of $J_{h,V}$ instead of J_V amounts only to 0.6 m and is accompanied by an increase in airspeed difference of 0.6 kt. These relatively small alterations in airspeed and altitude differences are due to the small differences in wind speed components, derived with the different objective functions. It has to be stressed that the iteration for the runs with the maximum difference in estimated wind speed components is displayed in figure 5. The remaining mean differences in speed and altitude in figure 5 are below airspeed and GPS measurement accuracies of 1 kt and 1.5 m respectively.

The wind estimated is almost independent of the objective functions used. Adding the altitude difference explicitly to the weighted sum of the objective function does only lead to a slight increase in the resulting difference in altitude. It is to be tested if the wind estimation is independent of the optimizer used and if the local optimizer Nelder-Mead simplex finds the global optimum when provided with a carefully chosen starting point.

7.2 Comparison of Optimizers

For the derivation of the SCADS1 as well as the calculation of the SCADS2 correction coefficients, both the simplex optimization routine and the evolutionary algorithm described above are used. In figure 6, the optimization iterations for the wind parameters V_{WN} , V_{WE} and V_{WD} calculated via the SCADS1 approach for the first windbox are displayed. In figure 7, the optimization iterations for the wind parameters $V_{WN,Wbox1}$, $V_{WE,Wbox1}$, the first two of the eight wind parameters of the SCADS2 approach, applied to the first windbox

set, are shown. The titles of each of the four subfigures of the figures 6 and 7 list the final values obtained with the applied optimizer in the unit kt. In the first subfigures of the figures 6 and 7, the final point of the evolutionary algorithm $V_{EA,end}$ which is the initial point of the Nelder-Mead simplex algorithm $V_{fmin,0}$ is marked with circles on each of the wind components to be optimized. As mentioned, the evolutionary algorithm runs 100 iterations for the SCADS1 method (figure 6) and 200 iterations for the SCADS2 (figure 7) method.

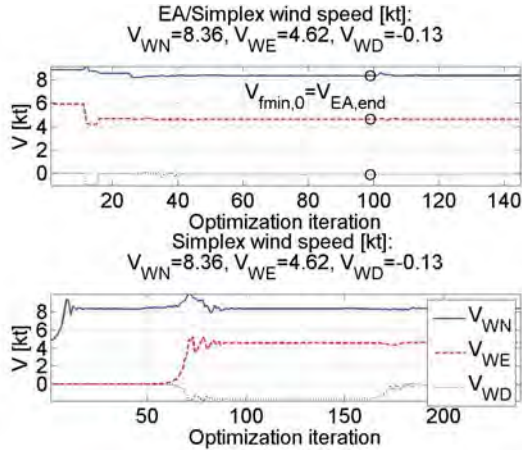


Figure 6: Progress of wind estimation at each SCADS1 iteration step: Evolutionary algorithm (EA) and simplex optimization for J_V

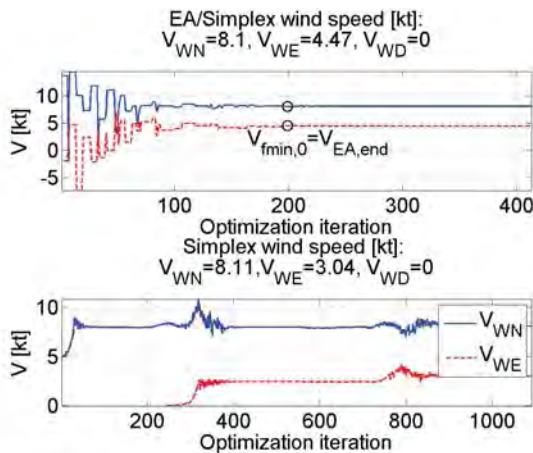


Figure 7: Progress of wind estimation at each SCADS2 iteration step: Evolutionary algorithm (EA) and simplex optimization for J_V

The starting point for the Nelder-Mead simplex is $\underline{x}_0 = [4.85, 0, 0]'$ kt. For the evolutionary algorithm, the displayed value is the value of the best individual of the respective generation. The starting point is hence the best individual of the randomly chosen first generation. The first generation consists of 30 starting points, individuals, which are randomly chosen within the following boundaries:

$$\text{SCADS1: } [10, 10, 1]' \geq \underline{x}_{i,0} \geq -[10, 10, 1]', \quad \underline{x}_{i,0} \in \mathbb{R}^3,$$

$$\text{SCADS2: } 10[\underline{1}] \geq \underline{x}_{i,0} \geq -10[\underline{1}], \quad \underline{x}_{i,0}, \underline{1} \in \mathbb{R}^8.$$

In the first subfigures displaying the hybrid optimization, the difference between the wind components found

by the evolutionary algorithm $V_{EA,end}$ and the final solution of the concatenation of the evolutionary algorithm and the simplex optimizer $V_{EA/fmin,end}$ is smaller than 0.01 kt. The maximum difference between the values found by the evolutionary algorithm does not exceed 0.5 kt for both methods. Although the change in wind parameters due to the simplex optimizer is small, this second step of the hybrid global optimizer evolutionary algorithm/simplex does indeed slightly improve the parameters found with the evolutionary algorithm.

For SCADS1, both the simplex optimizer and the evolutionary algorithm combined with a simplex optimization yield wind components equal to each other within a range of 0.03 kt. For all recorded 12 runs, the maximum difference in horizontal components does not exceed these values. The maximum difference in the downward component does not exceed 0.2 kt. The simplex optimization routine is able to find the same solution as the evolutionary algorithm, if applied to find an optimum dependent on three wind components from a starting point $\underline{x}_0 = [V_{WN,0}, V_{WE,0}, V_{WD,0}]$ within 9 kt difference to the final values $V_{WN,end,SCADS1}$, $V_{WE,end,SCADS1}$, $V_{WD,end,SCADS1}$.

If a combination of evolutionary algorithm and simplex optimizer is used to derive the SCADS2 wind components, the difference is less than 0.3 kt for all horizontal components to the components found by the SCADS1 method. As example, the final values of the SCADS2 run are shown in figure 7. In the first subfigure of figure 7 it can be deduced from the genes (the wind components) of the best individual of each iteration that the evolutionary algorithm searches a considerably wider variation of wind speeds than the simplex algorithm. As only the best individual is displayed, the wind speed components searched by the algorithm are likely to cover an even wider range than shown here. The minimum range of wind components searched has to be equal to the displayed of the best individual, though, and is thus considerably larger than the one considered by the simplex algorithm. The smaller wind speed range investigated by the Nelder-Mead simplex results in the algorithm getting stuck in local minima, when applied to estimate eight wind parameters.

The difference in resulting wind components obtained with the SCADS1 method with both optimizers are below the measurement accuracy of the ADS of 2 kt. The differences in the results obtained with the global hybrid optimization with the SCADS2 method closely resemble the results calculated with the SCADS1 method. This strongly suggests that the derived wind components are the best suitable parameters for the applied wind model of the wind acting on the helicopter during the flight. The noseboom correction coefficients are derived analytically from these wind components.

Differences in correction coefficients due to the different objective functions are discussed in the following section.

8 CORRECTION COEFFICIENTS

The pressure correction coefficients C_{P0} and C_{P1} , appearing in equation (4), and the ones for the airflow angles, C_{A0} , C_{A1} , C_{B0} and C_{B1} , from equations (1) and (2), are derived via estimated wind speed. The results obtained with the SCADS1 method and the three different objective functions are presented in subsection 8.1. For all tower flybys, wind measurements from an anemometer near the airport tower are available. As the tower flybys are flown under calm weather condition at an altitude of only 10 m over the runway surface, the measured wind should be a good estimate of the actual wind acting on the helicopter. Corrected noseboom airspeed, corrected with correction coefficients calculated with estimated wind, is compared to airspeed derived with measured wind in subsection 8.2.

8.1 Coefficients Derived with Estimated Wind

The mean values are displayed in table 2 for J_V , $J_{h,V}$ and $J_{P,\alpha,\beta}$. The standard deviations of these results are discussed in detail in [5].

	C_{P0} [Pa]	C_{P1} [-]	C_{A0} [rad]	C_{A1} [-]	C_{B0} [rad]	C_{B1} [-]
J_V	60.87	.1405	.0154	.7614	-.0205	.7730
$J_{h,V}$	80.18	.1144	.0132	.7585	-.0226	.7829
$J_{P,\alpha,\beta}$	74.87	.1302	.0252	.7527	-.0196	.7782

Table 2: SCADS mean values, derived with different objective functions

From the little difference in wind components it is expected that the correction coefficients resemble each other. This is true for the airflow correction coefficients: The mean values for the airflow correction multiplication coefficients C_{A1} and C_{B1} differ by less than 1.3% of the respective minimum value for all three objective functions. The absolute difference in offsets in the bias coefficients C_{A0} and C_{B0} is less than 0.7° and 0.2° , respectively.

However, although the difference in wind components is smaller than the measurement accuracy of the ADS, the mean values of the pressure correction coefficients derived for J_V differ by 30% from the mean values of $J_{h,V}$ and by 23% from the mean values of $J_{P,\alpha,\beta}$. To be able to judge the reason for these differences in the determined pressure correction coefficients, their influence on the resulting airspeed is investigated. The constant bias C_{P0} can be identified best by using low velocities resulting in pressure measurement around 0 Pa, whereas the influence of the scale correction factor C_{P1} becomes more pronounced at higher speeds. This can be deduced from equation (5) relating the correction coefficients C_{P0} and C_{P1} , the measured and the corrected noseboom dynamic pressures P_{di} and $P_{d,NB}$. The dynamic pressure measured during the SCADS windbox flight tests varies from 50 Pa to 1500 Pa. The airspeed can be calculated based on equation (14). Therefore, with the air density set to $\rho = 1.225 \text{ kg/m}^3$, the difference in airspeed, based on the measured pressure of $P_{di} = 50 \text{ Pa}$ and the mean

pressure correction coefficients from table 2, is calculated as:

$$\begin{aligned}\Delta V_{50} &= V_{50,NB,J_V} - V_{50,NB,J_{h,V}} \\ &= 27.34 \text{ kt} - 29.45 \text{ kt} = -2.08 \text{ kt}.\end{aligned}$$

This difference is an acceptable value for low airspeeds which are inherently difficult to measure. For the ADS, the measurement accuracy in this range is supposed to be 10 kt according to [11]. The speed difference decreases with increasing airspeed. The difference for a measured pressure of $P_{di} = 1500 \text{ Pa}$ is:

$$\begin{aligned}\Delta V_{1500} &= V_{1500,NB,J_V} - V_{1500,NB,J_{h,V}} \\ &= 106.44 \text{ kt} - 105.69 \text{ kt} = 0.76 \text{ kt}.\end{aligned}$$

This difference in airspeed due to the difference in correction coefficients is smaller than the ADS measurement accuracy. By increasing the influence of the height difference on the wind estimation, the airspeed accuracy is only slightly decreased within the range of 30 to 110 kt. The reference airspeed of the first windbox with airspeeds between 80 and 100 kt, derived from DGPS and estimated wind and denoted DGPS, is depicted in figure 8. The ADS airspeed and the noseboom airspeed, corrected with the correction coefficients listed for J_V and $J_{h,V}$ in table 2, are displayed as well.

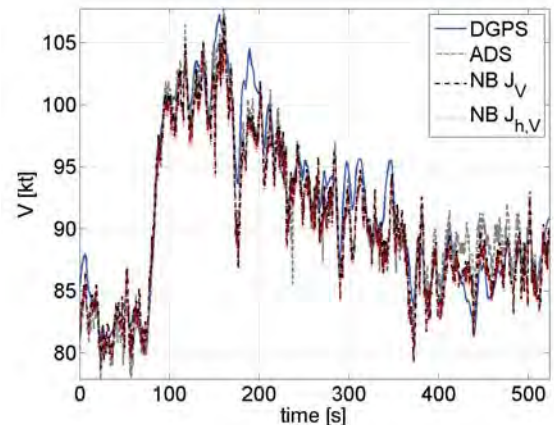


Figure 8: 1st windbox, 80 to 100 kt, reference airspeed (DGPS and estimated wind), ADS and noseboom airspeed, correction coefficients derived from J_V and $J_{h,V}$

The maximum difference here between the two differently corrected noseboom airspeeds is 0.31 kt and the mean deviation is 0.061 kt. The mean value of the difference between the airspeed and the corrected noseboom value is 0.60 kt and its standard deviation is 1.37 kt. Both correction sets, the one for J_V as well as the one for $J_{h,V}$, thus lead to a good fit to the ADS data. The peaks of up to 6 kt difference to the reference data from GPS and estimated wind are due to wind gusts which are not modeled with the constant wind model.

In figure 9 the difference of the ADS and the two corrected noseboom airspeeds to the reference airspeed is shown. Their respective mean difference to the reference airspeed is displayed in the subfigure titles. As almost no difference is calculated in the airspeed range of the first windbox based on the difference in correction factors from table 2, the altitude difference will not be decreased considerably by using the correction coef-

ficients obtained with the objective function $J_{h,V}$. The resulting altitude of the first windbox is shown in figure 10. In the second and the third subfigures the difference between the reference altitude and the altitude based on the corrected noseboom data is shown.

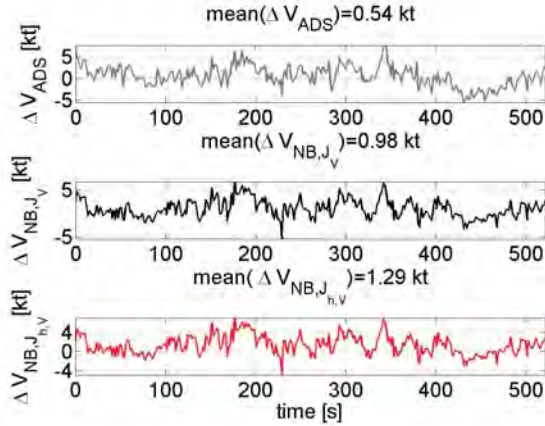


Figure 9: 1st windbox, difference to reference airspeed of ADS and noseboom airspeed, correction coefficients derived from J_V and $J_{h,V}$

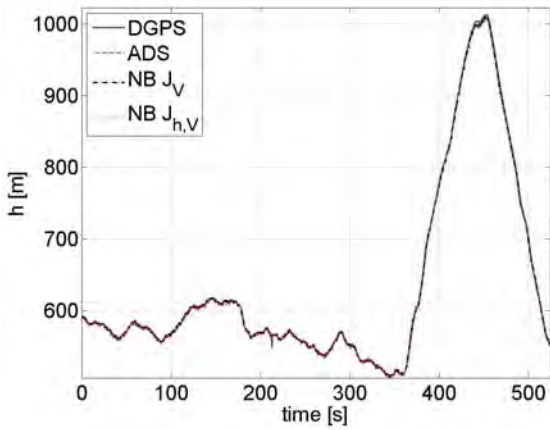


Figure 10: 1st windbox 80 to 100 kt, reference altitude (DGPS and estimated wind), ADS and noseboom altitude, correction coefficients derived from J_V and $J_{h,V}$

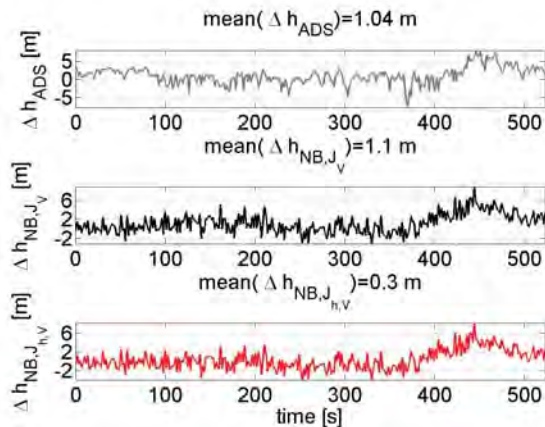


Figure 11: 1st windbox, difference to reference altitude of ADS and noseboom altitude, correction coefficients derived from J_V and $J_{h,V}$

In the first subfigure of figure 11 the difference between the reference altitude and the altitude derived based on

the ADS pressure is shown. The improvement due to the use of the objective function $J_{h,V}$ is close to the DGPS measurement accuracy and below the measurement accuracy of the INS/GPS system. The ADS airspeed is a good fit to the reference airspeed based on the estimated wind for airspeeds above 40 kt, figure 8 and figure 9.

At airspeeds below 30 kt the rotor downwash negatively influences the ADS measurement, figure 12.

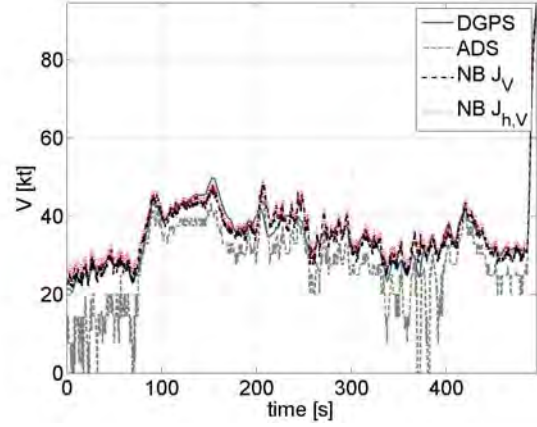


Figure 12: 4th windbox 20 to 40 kt, reference airspeed (DGPS and estimated wind), ADS and noseboom airspeed, correction coefficients derived from J_V and $J_{h,V}$

In the first subfigure of figure 13 the difference between reference airspeed and ADS airspeed is displayed. In the second and the third subfigure the noseboom data corrected with J_V and the noseboom data corrected with $J_{h,V}$ are depicted.

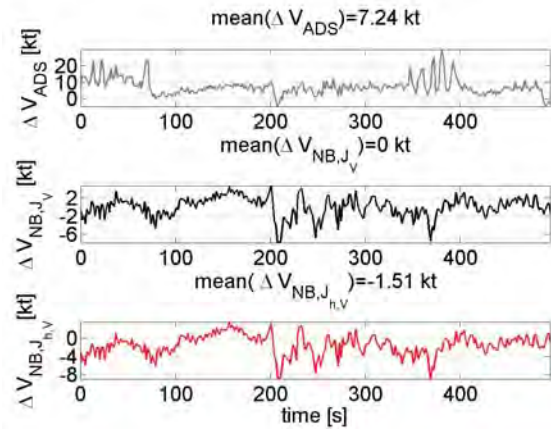


Figure 13: 4th windbox, difference to reference airspeed of ADS and noseboom airspeed, correction coefficients derived from J_V and $J_{h,V}$

Considering the differences ΔV_{1500} and ΔV_{50} , the difference between the airspeeds V_{NB,J_V} and $V_{NB,J_{h,V}}$ is more pronounced at lower airspeeds, which corresponds to the difference in mean values in the figures 9 and 13. Applying the objective function J_V leads to a smaller difference to the reference airspeed at lower airspeeds and only to a slight increase in altitude error.

In [5] it is discussed in detail, that for the airspeed range flown in the SCADS windboxes, the values C_{P0} and C_{P1} are linearly dependent on each other. The bias correction coefficient C_{P0} decreases with increasing C_{P1} .

The same trend can be seen in table 2. If the bias correction coefficient is fixed to the value $C_{P0} = 60.87$ Pa derived with the objective function J_V , the following multiplication correction coefficients are derived with the three objective functions:

$$\begin{aligned} C_{P1}(J_V) &= .1406, \\ C_{P1}(J_{h,V}) &= .1412, \\ C_{P1}(J_{P,\alpha,\beta}) &= .1527. \end{aligned}$$

The difference between the factors $(1 + C_{P1}(J_V))$ and $(1 + C_{P1}(J_{P,\alpha,\beta}))$ with which the dynamic pressure is multiplied to calculate the corrected noseboom airspeed amounts to 1%. Hence, the accuracy loss due to differences in correction factors is for the high airspeed range smaller than 1.5 kt for all airspeeds below 150 kt if the bias correction coefficient is fixed.

Apparently, the linear dependency between C_{P0} and C_{P1} for the SCADS1 approach was caused by too little airspeed variation within the windbox. Therefore it is tested if a method taking into account a wider range of airspeeds, i.e. more information than can be provided by the windbox maneuvers, can narrow the variance in both coefficients.

As was mentioned before, the bias C_{P0} has to be determined at low airspeeds. Therefore, the coefficients derived using estimated wind and SCADS windboxes are tested against measured wind and tower flybys varying from 5 to 80 kt. A comparison between mean values of differences between reference and corrected noseboom data for four SCADS windboxes and the three faster pace car runs is shown in table 3.

Windbox V_{lo}	80 kt	60 kt	40 kt	20 kt
	[kt]	[kt]	[kt]	[kt]
$\Delta V_{TAS} J_V$	0.98	0.66	1.85	0.00
$\Delta V_{TAS} J_{h,V}$	1.29	0.75	2.36	1.51

Flyby V_{const}	16.2 kt	21.6 kt	27.1 kt
	[kt]	[kt]	[kt]
$\Delta V_{TAS} J_V$	1.16	1.75	1.94
$\Delta V_{TAS} J_{h,V}$	4.27	4.27	2.52

Table 3: Mean differences between reference and noseboom airspeed for different maneuvers and different objective functions

The reference airspeed is calculated with DGPS and estimated wind for the four SCADS windboxes. The reference airspeed is calculated with DGPS and measured wind for the three tower flybys. The two sets of calibration results, based on the objective functions J_V and $J_{h,V}$ show good fits for the windboxes with nominal speeds from 20 to 90 kt and a maximum speed of 110 kt. The values of the SCADS1 J_V set show smaller differences when applied at low airspeed i.e. 16.2 kt to 30 kt, though. Apparently, the bias value $C_{P0}(J_V)$ is a good fit for low velocities as well.

8.2 Coefficients Tested Using Measured Wind

The wind measured during tower flyby tests by an anemometer mounted near the airport tower has to

be subtracted from the measured ground speed of the helicopter. In [5] it is demonstrated that correction coefficients derived from measured wind agree relatively well with correction coefficients derived from estimated wind. Here, the measured wind is only used to validate the correction coefficients derived via estimated wind.

The correction coefficients obtained with $J_{h,V}$ lead to an increased difference in airspeed for the lower airspeeds, as was shown in table 3. It is to be tested if the difference in height to the reference data can be decreased by using this function as a compensation for the loss in airspeed accurateness. Figure 14 shows the application of the correction parameters to data from a deceleration tower flyby.

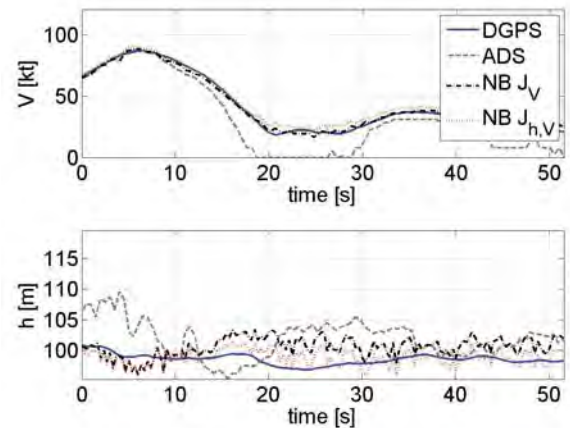


Figure 14: Deceleration tower flyby 20 to 80 kt, reference (DGPS and measured wind), ADS and noseboom airspeed and altitude, correction coefficients derived from J_V and $J_{h,V}$

The reference airspeed is GPS ground speed subtracted by measured wind. At airspeeds higher than 60 kt, the GPS based airspeed and the ADS measurements agree well. The differences between air data system and reference airspeed increase considerably for airspeeds lower than 60 kt.

For all airspeeds below 60 kt, noseboom airspeed provides the only reliable, online-available airspeed data. Moreover, figure 14 shows that the difference to the reference speed is smaller at lower airspeed if the noseboom is corrected with values derived with J_V as objective function. It has to be determined down to which airspeed valid noseboom data can be obtained. For this purpose, the low speed pace car flight tests are undertaken.

The pace car flybys were used to identify the lowest speed at which valid noseboom measurements are still available. Figure 15 shows the resulting dynamic pressures and velocities for the third pace car run at 20 km/h (10.4 kt) and figure 16 for the fourth run at 30 km/h (16.2 kt).

The noseboom measurements are corrected with the mean values derived with coefficients from wind estimated by optimizing J_V and by optimizing $J_{h,V}$. When the air data measurement system, mounted below the

helicopter, is corrupted by rotor downwash, the dynamic pressure measurements become negative. For this case, a velocity of zero is indicated by the air data system. The corrected noseboom dynamic pressure is close to zero, but not negative. Still, as the downwash influences the noseboom measurement, too, these measurements at an airspeed of 10.8 kt are very noisy.

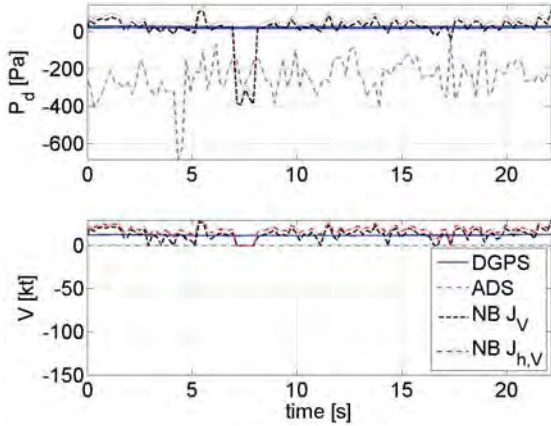


Figure 15: Pace car flyby 10.3 kt, reference (DGPS and measured wind), ADS and noseboom dynamic pressure and airspeed, correction coefficients derived from J_V and $J_{h,V}$, invalid noseboom measurement

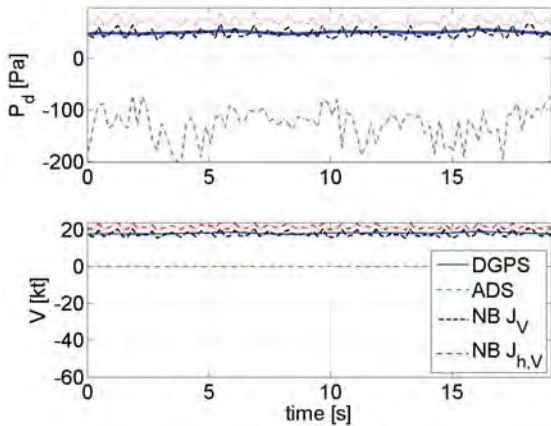


Figure 16: Pace car flyby 16.2 kt, reference (DGPS and measured wind), ADS and noseboom dynamic pressure and airspeed, correction coefficients derived from J_V and $J_{h,V}$, valid noseboom measurement

At 16.2 kt, depicted in figure 16, it can be seen that the airspeed of the noseboom, corrected with the values obtained with the objective function J_V , is a good match to the reference airspeed. The values of the objective function $J_{h,V}$ show larger deviation to the reference airspeed.

The overall discrepancies to the reference height are slightly smaller if the correction set $J_{h,V}$ is used: the overall mean values of the difference to DGPS values for the last three runs is 0.17 m instead of 1.48 m, see figure 17. As the airspeed correction is considerably better with the parameters obtained with J_V with a relative small difference to the reference height data, this parameter set is chosen as the correction parameters.

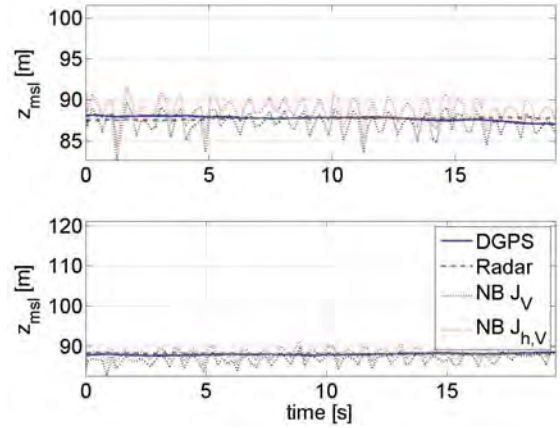


Figure 17: Altitude at pace car flyby, 1st subfigure: airspeed 16.2 kt, 2nd subfigure: airspeed 21.6 kt

It has to be stressed that at the airspeed of 16.2 kt the pitot tube of the basic ADS is still influenced by rotor downwash and yields negative, invalid dynamic pressure and no airspeed. On the other hand, measured dynamic pressure corrected with the J_V values gives a good fit of noseboom speed to reference airspeed.

9 CONCLUSION

The SCADS (Simultaneous Calibration of Air Data Systems) technique has been used to dynamically calibrate the noseboom measurements of the EC135 FHS of DLR. Both the pressure measurements from the pitot system and the airflow angle values from the airflow vanes are calibrated with estimated wind.

In the absence of measured wind to validate the estimations, they are carried out with three different objective function and two optimizers. The first objective function J_V weights the difference between reference and noseboom airspeed components. The second objective function $J_{h,V}$ additionally weights the altitude difference. The third function $J_{P,\alpha,\beta}$ directly uses the dynamic pressure and airflow measurements. The results show that:

- the mean difference in estimated wind components as a result of different objective functions is smaller than 0.7 kt for all wind components
- the maximal difference due to the difference between local and global optimizer is smaller than 0.03 kt for the two horizontal and 0.2 kt for the vertical wind component

The estimated wind is thus deemed the best possible fit for the applied wind model of the wind acting on the helicopter. Therefore, it can be further concluded that:

- optimizing the sensor correction coefficients with reference to J_V leads to good matches both to the reference airspeed as well as to the reference height

The calculated signals, derived with the identified correction terms, provide the desired accuracy and widen the range in which airspeed can be detected via dynamic pressure measurements from the measurement range of 30 to 110 kt to 16.2 to 110 kt.

REFERENCES

- [1] K. Hui, S. Baillie: *Validation of the Simultaneous Calibration of Aircraft Position Error and Airflow Angles Using a Differential GPS Technique on a Helicopter*, AGARD FVP Symposium on Advances in Flight Testing, Lisbon, 1996
- [2] K. Hui: *Application of the Simultaneous Calibration of Aircraft Position Error and Airflow Angles Using a Differential GPS Technique on a Bell 212 Helicopter*, Laboratory Memorandum, Institute for Aerospace Research, Flight Research Laboratory, NRC, Ottawa, 1998
- [3] B. Leach, K. Hui: *In-flight Technique for Calibrating Air Data Systems Using Kalman Filtering and Smoothing*, AIAA Atmospheric Flight Mechanics Conference, Montreal, 2001
- [4] V. Parameswaran, R. Jategonkar, M. Press: *Five-Hole Flow Angle Probe Calibration from Dynamic and Tower Flyby Maneuvers*, Journal of Aircraft, Vol. 42, No.1, January-February, 2005
- [5] A. Dittmer, S. Seher-Weiß: *Dynamic Calibration of the Noseboom Sensors of the Flying Helicopter Simulator FHS*, DGLR Deutscher Luft und Raumfahrtkongress, Hamburg, 2010
- [6] S. Seher-Weiß: *Kompatibilitätskontrolle und Nasenmastkalibrierung*, Institutsbericht IB 11-2009/31, DLR, Braunschweig, 2009
- [7] N. N.: *Technical Data for Universal Nose Data Boom SAC P/N 100510 and Accessory*, SpaceAge Control Inc., 1997
- [8] N. N.: *SHARPE XR6 (including RPS), GPS Receiver, User Manual*, Symmetricom Ltd
- [9] N. N.: *Windrichtungsgeber*, Thies Clima, Bedienungsanleitung 020889/11/07, 2007
- [10] N. N.: *Prime Item Development Specification for the H-764GU GATM Upgrade Embedded GPS/INS, Specification No. DS 34209200 Rev F*, 2002
- [11] P. Guichard: *ADS3000 System Requirement Document DLR03*, Sextant Avionique, 1997
- [12] H. Schlichting, E. Truckenbrodt: *Aerodynamik des Flugzeuges*, Erster Band, Springer, 1967
- [13] J. Lagarias, J. Reeds, M. Wright, P. Wright: *Convergence Properties of the Nelder-Mead Simplex Method in Low Dimensions*, SIAM Journal of Optimization, Vol. 9 Number 1, pp. 112-147, 1998.
- [14] R. Storn: *Differential Evolution Research - Trends and Open Questions in Differential Evolution Research*, U. K. Chakraborty, editor, Advances in Differential Evolution, chapter 1, Springer, 2008